

Observation of soft x rays of single-mode resonant transition radiation from a multilayer target with a submicrometer period

Koji Yamada* and Teruo Hosokawa

NTT System Electronics Laboratories, 3-1 Morinosato-Wakamiya, Atsugi 243-0198, Japan

Hisataka Takenaka

NTT Advanced Technology, 1-1-3 Gotenyama, Musashino 180-8639, Japan

(Received 2 October 1998)

The soft x rays produced by resonant transition radiation from a multilayer target with a submicrometer period were measured. The target consisted of 176-nm-thick nickel as radiators and 221-nm-thick carbon as spacers alternately stacked on a SiN membrane. The target was bombarded by 15-MeV electrons, and the angular dependence of the resulting x-ray spectra was measured. The spectra had a clear single peak at energies from 2 to 4 keV depending on the observation angle. The spectral dependence on the incident angle of the electron beam was also measured, and a shift of the peak energy was observed. These experimental results showed a good agreement with theoretical estimations. These results are clear evidence of single-mode resonant transition radiation. [S1050-2947(99)01705-9]

PACS number(s): 79.20.Kz, 41.75.Ht, 07.85.-m, 78.70.-g

I. INTRODUCTION

Brilliant and tunable x-ray sources are being used in various research fields, and in the near future they are expected to be applied even to industrial uses. Presently, synchrotron radiation (SR) is the unique x-ray source that satisfies both brilliance and tunability; however, the high cost and large size of SR facilities create serious inconvenience in using them.

To eliminate the inconvenience, we have been studying transition radiation (TR) as a compact x-ray source. This radiation is emitted when high-energy electrons pass through the interface between materials with different dielectric constants [1]. The photon energy of TR is nearly $\gamma\hbar\omega_p$, where γ is the Lorentz factor of the electrons and ω_p is the plasma frequency of the materials. The radiation is collimated forward within an emission angle of about $1/\gamma$ with respect to the trajectory of the electrons. TR has potential as a compact x-ray source because the electron energy needed to emit x rays by TR is far lower than that by SR. It is also an advantage of TR that its photon yield per electron is far larger than that of SR [2].

Transition radiation from only one interface, however, does not have sufficient monochromaticity, intensity, and tunability for a future x-ray source. These characteristics can be improved by using a periodic interface structure, which creates a strong interference effect. For example, if x-ray absorption in the target itself is neglected, the x-ray spectrum shows a sharp peak whose bandwidth of $\omega/\delta\omega$ is about equal to the periodicity number of the target, N . The interference effect also gives us an easy tuning method. The peak energy varies with the emission angle because of the change in interference conditions. The interfered TR was first described

by Ter-Mikaelyan [3] and is called resonant transition radiation (RTR).

To better understand the characteristics of RTR, many experiments have been performed by various groups. In most of these experiments, however, the resonance effect was not well observed because the divergence of the electron beams was larger than the collimation angle of about $1/\gamma$. As a result, the measured x-ray spectrum was a convolution of the spectra for various emission angles, and the angular dependence of the RTR spectrum disappeared [2]. This is an extremely serious problem which has come up in experiments that use over-GeV electrons. Even in the few experiments in which the angular dependence of the x-ray spectra was measured, the spectra contained many peaks of higher harmonic modes [4,5]. This problem originates from the difficulty in manufacturing a stacked target with narrow vacuum spacings.

To overcome these problems and to confirm the generation of single-mode RTR, we used medium-energy (15 MeV) electrons and a multilayer target with a submicrometer period.

II. THEORETICAL APPROACH TO THE SINGLE-MODE RTR

The differential photon yield of single-interface TR per solid angle per electron is given by [6,7]

$$\frac{d^2N_0}{d\Omega d\omega} = \frac{\alpha\omega \sin^2\theta}{16\pi^2c^2} (Z_1 - Z_2)^2, \quad (1)$$

where N_0 is the number of photons emitted at angle θ with respect to the electron trajectory, ω is the angular frequency of the radiation, and α is the fine-structure constant. Z_1 and Z_2 are the formation lengths of media 1 and 2:

*Author to whom correspondence should be addressed. FAX: +81-462-40-4324. Electronic address: kyamada@aec1.ntt.co.jp

$$Z_i \cong \frac{4c\beta}{\omega[\gamma^{-2} + (\omega_i/\omega)^2 + \theta^2]}, \quad (2)$$

where ω_i is the plasma frequency of the media. For a periodic stack of N foils with thickness l_1 and spacing l_2 , the differential yield is given by [8]

$$\frac{d^2 N_p}{d\Omega d\omega} = \frac{d^2 N_0}{d\Omega d\omega} F_1 F_N, \quad (3)$$

where F_1 represents the *inner-foil* resonance,

$$F_1 = 1 + \exp(-\mu_1 l_1) - 2 \exp(-\mu_1 l_1/2) \cos\left(\frac{2l_1}{Z_1}\right), \quad (4)$$

and F_N represents the *inter-foil* resonance,

$$F_N = \frac{1 + \exp(-N\sigma) - 2 \exp(-N\sigma/2) \cos(2NX)}{1 + \exp(-\sigma) - 2 \exp(-\sigma/2) \cos(2X)}, \quad (5)$$

where $\sigma = \mu_1 l_1 + \mu_2 l_2$, $X = l_1/Z_1 + l_2/Z_2$. μ_1 and μ_2 are the x-ray-absorption coefficients of each medium.

From the equations for F_1 and F_N , we can derive the resonance conditions of RTR:

$$\frac{l_1}{Z_1} = \frac{2n-1}{2} \pi \quad (6)$$

and

$$X = \frac{l_1}{Z_1} + \frac{l_2}{Z_2} = m\pi, \quad (7)$$

where n and m are integers. To obtain a single-peak x-ray spectrum, the resonance conditions should be $n=1$ and $m=1$ at the x-ray energy near $\gamma\hbar\omega_p$. In other words,

$$\frac{l_1}{Z_1} = \frac{l_2}{Z_2} = \frac{\pi}{2}. \quad (8)$$

This condition means that the photon energy of the fundamental harmonic mode is about $\gamma\hbar\omega_p$. The energies of higher harmonic modes are a few or more times larger than that of the fundamental harmonic mode; however, the yields of the higher harmonic mode are far lower than that of the fundamental harmonic mode. This is because the yield of RTR at over an energy of $\gamma\hbar\omega_p$ drops rapidly to very small values [6]. Thus, only the fundamental harmonic mode can survive. As an example, the solid line in Fig. 1 shows the calculated spectrum of the single-mode RTR. A large 2.2-keV peak appears at an emission angle of 34 mrad when a stacked target consisting of ten pairs of 185-nm nickel foil and 243-nm vacuum spacing is bombarded by 15-MeV electrons. The second harmonic peak is as small as one-hundredth of the fundamental harmonic peak.

As mentioned above, to satisfy the single-mode condition, the thicknesses of the foils and spacings must be of the order of micrometers or less. In conventional targets consisting of thin foils and vacuum spacings, however, the spacings have typically been more than a few tens of micrometers [8] because it is difficult to manufacture targets with submicrome-

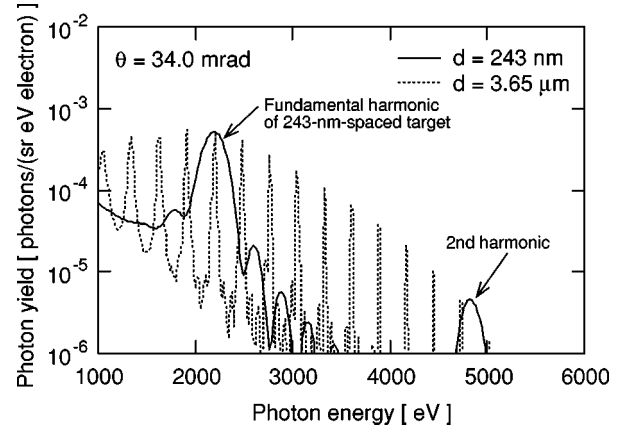


FIG. 1. Dependence of calculated RTR spectra on thickness of spacings. The target consisted of ten foils of 185-nm-thick Ni.

ter vacuum spacings. When large spacings are used, the energy of the fundamental harmonic mode is in an energy region far lower than that of x rays. Therefore, the energy intervals of the higher harmonic modes become narrow, and many peaks appear in the x-ray region. As an example, the dotted line in Fig. 1 shows a calculated spectrum for such a multimode RTR. Except for the spacing, the calculation conditions are the same as those used for calculating the single-mode RTR spectrum. The spacing is 3.65 μm , which is 15 times larger than that of the single-mode RTR. As a result, many peaks appear in the x-ray region from 1 to 5 keV. This multimode effect is the reason why RTR spectra have had many peaks in the x-ray region even in experiments with fine angular resolution.

III. EXPERIMENTAL SETUP

A. Multilayer target

The most important element in our experimental setup is the multilayer target. It consists of 176-nm-thick nickel (Ni) radiator layers and 221-nm-thick carbon (C) spacer layers. These layers were alternately deposited by RF magnetron sputtering on a silicon-nitride (SiN) membrane. The structure of the target is shown in Fig. 2. The standard deviations of the thicknesses of these layers were about 3.3%. We used Ni for the radiator material because of its high TR yield and its transparency for keV-region x rays. We used carbon for

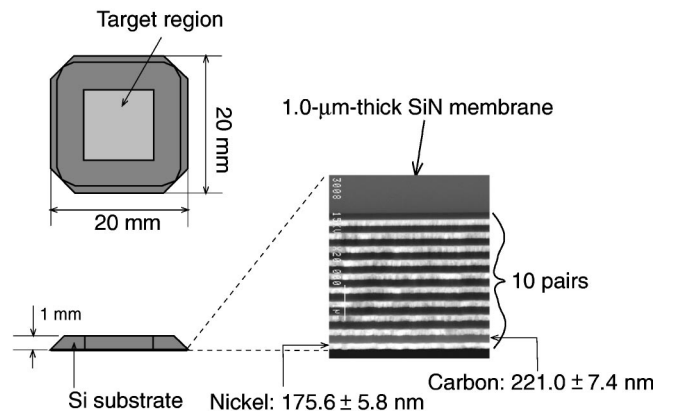


FIG. 2. Ni/C multilayer target.

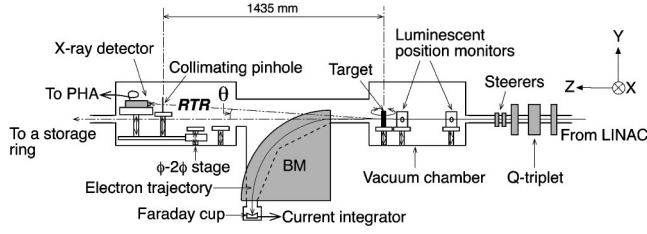


FIG. 3. Experimental setup for RTR measurement.

spacers because of its high x-ray transparency. The transparency data of these materials are given in Ref. [9].

The thicknesses of these layers are such that the target bombarded by 15-MeV electrons should emit 2.2-keV photons at an emission angle of 34 mrad. The target should also emit 2.93- and 3.77-keV photons at 25.5- and 17.0-mrad emission angles, respectively. The second harmonic modes, whose yields should be about one-hundredth of that of the fundamental harmonic mode, are estimated to be 5.00, 6.60, and 8.09 keV for 34.0-, 25.5-, and 17.0-mrad observation angles, respectively.

B. Apparatus

The experimental system is located at the NTT SR facility [10]. The electron source is a LINAC [11], which is usually used as an injector for storage rings. A schematic of the system is shown in Fig. 3. The electron energy of the LINAC was 15 MeV, and its energy deviation was about 1% full width at half maximum (FWHM). The LINAC generated beam pulses at 10-Hz repetition. The pulse width was about 2 ns, and each pulse contained about 1 pC charge. The amount of the charge per pulse was determined so that pile-up effects should be reduced. The electron beam was focused by a Q triplet and guided to the target. The beam parameters, such as the beam emittance, size, divergence, and incident angles, were measured by monitoring the luminescence emitted from the beam position monitors and the target holder. The measured phase-space map of the beam at the target is shown in Fig. 4.

The electrons passing through the target were bent by a bending magnet (BM) and guided to a Faraday cup, where beam charge was measured. Since the electrons pass through the membrane before reaching the Ni/C part of the target, the membrane has a negligible effect on the radiation. The RTR passed through a 1-mm ϕ collimating pinhole made of

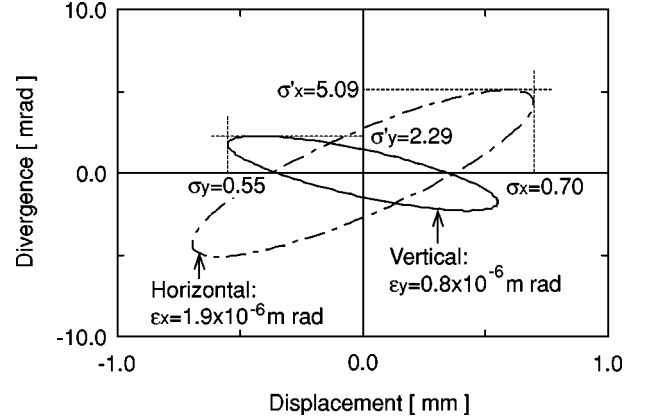


FIG. 4. Phase space map of the electron beam at the target. The map shows the contours at the standard deviations of the electron distributions.

1-mm-thick aluminum and was detected by a Si-PIN diode detector [12] with a 13- μ m-thick beryllium (Be) window. The distance from the target to the pinhole was 1435 mm. The detector was connected to a multichannel pulse-height analyzer (MCA). The detector was calibrated by K edge x rays of Si and Ti, and its energy resolution was measured to be about 300-eV FWHM. To eliminate incorrect events due to the pile-up effects and environmental noises, the detector system was gated both by the pile-up signal from the pulse-shaping circuit and by the trigger of the LINAC gun. For measuring soft x rays and VUV, all of the equipment, except the magnets, was placed in a vacuum.

IV. ESTIMATION OF RTR SPECTRA

A. Degradation of measured RTR spectra

Prior to measuring RTR spectra, we have to consider how the various factors of the experimental environment degrade the spectra. The most serious degradation is the broadening of the peak width caused by variations in the observation angle. These variations originate mainly from divergence of the electron beams. The beam size at the target and the aperture of the collimating pinhole also cause angular variations. These variations cause the detector to see x rays with various emission angles with respect to the trajectories of each electron. The measured x-ray spectrum should therefore be a convolution of the spectra for various emission angles. Considering this effect, the differential yield at a geometrical observation angle of θ_0 is

$$\frac{d^2 N_{p:\text{ang}}}{d\Omega d\omega} = \frac{1}{2\pi\delta\theta_x\delta\theta_y} \int_{\theta_x=-3\delta\theta_x}^{+3\delta\theta_x} \int_{\theta_y=\theta_0-3\delta\theta_y}^{\theta_0+3\delta\theta_y} \exp\left[-\left\{\frac{(\theta_y-\theta_0)^2}{2\delta\theta_y^2} + \frac{\theta_x^2}{2\delta\theta_x^2}\right\}\right] \frac{d^2 N_p(\theta \rightarrow \sqrt{\theta_x^2 + \theta_y^2})}{d\Omega d\omega} d\theta_y d\theta_x, \quad (9)$$

where $\delta\theta_x$ and $\delta\theta_y$ are the half-widths of the transverse angular variations in the horizontal and vertical directions, respectively. For simplicity, we assume here that the electron beams have Gaussian distributions in the (x, x', y, y') phase space. The expression $\theta \rightarrow \sqrt{\theta_x^2 + \theta_y^2}$ means that variable θ is

replaced by $\sqrt{\theta_x^2 + \theta_y^2}$. Since the integration limits are set to be $\pm 3\delta\theta$, the 99.7% of electrons in the beams are taken into account in these convolution processes.

We must also consider the x-ray absorption in the detector window and how the wavelength resolution of the detector

TABLE I. Results of fitting RTR spectra to Gaussian function.

			θ_0 (mrad)			
			17.0	25.5	34.0	25.5 (slant incidence)
Theoretical (ideal)	$10^2 S_0$	[photons/(sr el.)]	3.551 ± 0.051	6.524 ± 0.083	7.523 ± 0.120	7.925 ± 0.11
	ϵ_0	(eV)	3768.0 ± 2.8	2929.0 ± 2.1	2185.4 ± 2.4	2562.9 ± 2.3
	σ_ϵ	(eV)	168.2 ± 2.8	142.1 ± 2.1	128.9 ± 2.4	139.9 ± 2.3
	correlation coeff.		0.9826	0.9870	0.9800	0.9842
Theoretical (degraded)	$10^2 S_0$	[photons/(sr el.)]	3.673 ± 0.025	6.494 ± 0.038	7.156 ± 0.035	7.749 ± 0.045
	ϵ_0	(eV)	3663.0 ± 3.1	2875.6 ± 2.5	2173.7 ± 2.0	2522.9 ± 2.5
	σ_ϵ	(eV)	387.5 ± 3.1	375.0 ± 2.5	346.3 ± 2.0	363.7 ± 2.5
	correlation coeff.		0.9912	0.9939	0.9958	0.9939
Experimental	$10^2 S_0$	[photons/(sr el.)]	3.695 ± 0.092	4.322 ± 0.106	3.987 ± 0.123	3.986 ± 0.114
	ϵ_0	(eV)	3531.5 ± 13.0	2853.4 ± 11.2	2128.8 ± 14.2	2459.9 ± 15.2
	σ_ϵ	(eV)	455.2 ± 13.0	394.5 ± 11.2	396.6 ± 14.2	461.4 ± 15.2
	correlation coeff.		0.9753	0.9752	0.9597	0.9630

broadens the peak width. The detection efficiency does not have to be considered here because it is almost 100% for 2- to 4-keV x rays. Considering these factors, the RTR spectrum to be obtained in our experiments can be expressed as

$$\frac{d^2 N_{p:\text{exp}}}{d\Omega d\omega} = \frac{1}{\sqrt{2\pi}\sigma_d} \int_{\omega'=0}^{\infty} \exp\left\{-\frac{(\omega' - \omega)^2}{2\sigma_d^2}\right\} \times \exp(-\mu_d l_d) \frac{d^2 N_{p:\text{ang}}}{d\Omega d\omega} d\omega', \quad (10)$$

where σ_d , μ_d , and l_d are the standard deviation of the detector's wavelength resolution, the absorption coefficient of the window material, and the thickness of the window, respectively.

B. Estimated spectra

Given the beam sizes and divergences shown in Fig. 4 and considering the geometry of our measurement system, the angular variations were calculated to be $\delta\theta_x \approx 5.9$ mrad and $\delta\theta_y \approx 3.0$ mrad. The detector had 13- μm -thick Be, and σ_d was about 130 eV. Using these values, we calculated the RTR spectra to be obtained in our experiments. For quantitative analysis, we fitted the calculated spectra by the Levenberg-Marquardt method on a Gaussian function,

$$f(S_0, \epsilon_0, \sigma_\epsilon) = \frac{S_0}{\sqrt{2\pi}\sigma_\epsilon} \exp\left\{-\frac{(\epsilon - \epsilon_0)^2}{2\sigma_\epsilon^2}\right\}, \quad (11)$$

where ϵ , ϵ_0 , and σ_ϵ are the variables representing the photon energy, the peak energy, and the standard deviation of the peak widths, respectively. S_0 is the total number of photons in a peak. Note here that the FWHM bandwidth can be calculated as $2.35\sigma_\epsilon$. The fitted results and the correlation coefficients are listed in Table I.

Figures 5(a) and 5(b) show the calculated spectra at $\theta_0 = 17.0, 25.5,$ and 34.0 mrad. When the degradation is not considered, as shown in Fig. 5(a) and listed in the upper part

of Table I, the spectra have narrow peaks with FWHM bandwidths of about 350 eV. Because of the x-ray absorption in the target itself, the FWHM values are a bit larger than that without considering the absorption. We can also see the shift of the peak energy with respect to the change in the observation angle. No peak of the second harmonic mode can be seen.

When the degradation is considered, as shown in Fig. 5(b) and listed in the middle part of Table I, the FWHM bandwidths increase to about 880 eV and the peaks become lower. Even though the spectra are degraded, each peak is still able to be discriminated clearly. Our experimental apparatus can therefore be used to observe the resonance effect of single-mode RTR.

We also calculated the effect of changing the incident angle of the electron beams. The electrons with slant incidence travel thicker layers than those with normal incidence;

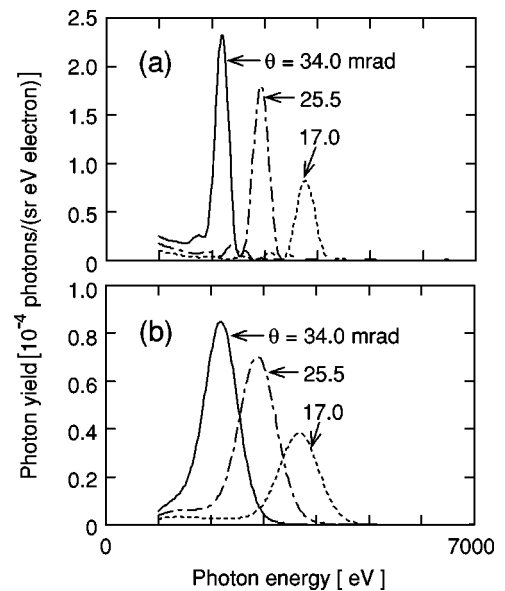


FIG. 5. Dependence of calculated RTR spectra on emission angle: (a) without degradation and (b) considering degradation.

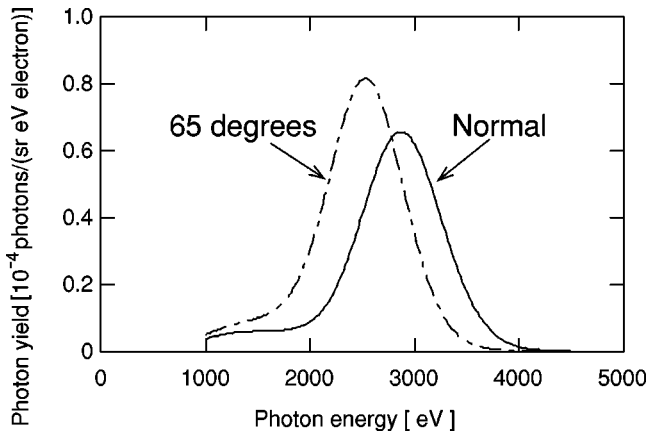


FIG. 6. Dependence of calculated RTR spectra on incident angle of electrons.

herefore, the resonance condition should change. The calculated RTR spectra for incident angles of 90° (normal) and 65° at $\theta_0 = 25.5$ mrad are shown in Fig. 6. They include the effects of degradation. The spectrum peak for the slant incidence is 350 eV lower than that for the normal incidence. Although the peaks overlap, the 350-eV peak shift is large enough to discriminate them.

V. EXPERIMENTAL RESULTS

A. Dependence on observation angle

A target with ten pairs of Ni/C layers was bombarded normally by 15-MeV electrons, and the energy spectra of the resulting x rays were measured. The characteristics of the electron beams were the same as those described above. To measure the dependence of RTR spectra on the observation angle, the photons from the target were measured at the observation angle of 17, 25.5, and 34 mrad with respect to the beam trajectory. These angles ranged from $1/2\gamma$ to $1/\gamma$. The angles were selected by changing the vertical position of the collimating pinhole. The background spectra were also measured by using a target consisting of a $2\text{-}\mu\text{m}$ -thick Ni foil and a $2\text{-}\mu\text{m}$ -thick carbon foil; their thicknesses were almost the same as the sums of those in the Ni/C multilayer target.

Figure 7 shows an example of the raw spectra measured at the observation angle of 25.5 mrad. The spectrum of the x

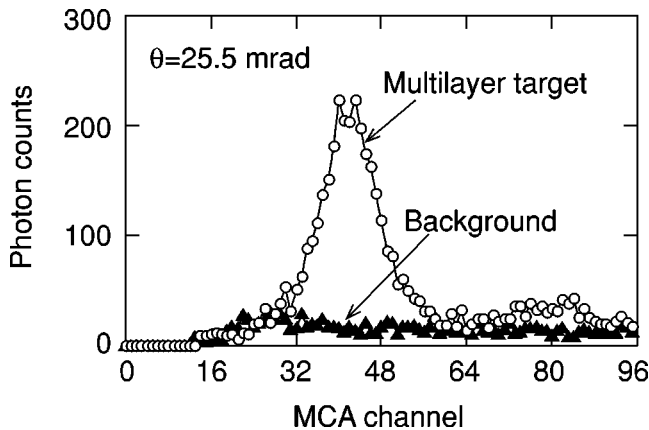


FIG. 7. An example of the raw data of the RTR spectrum measurements.

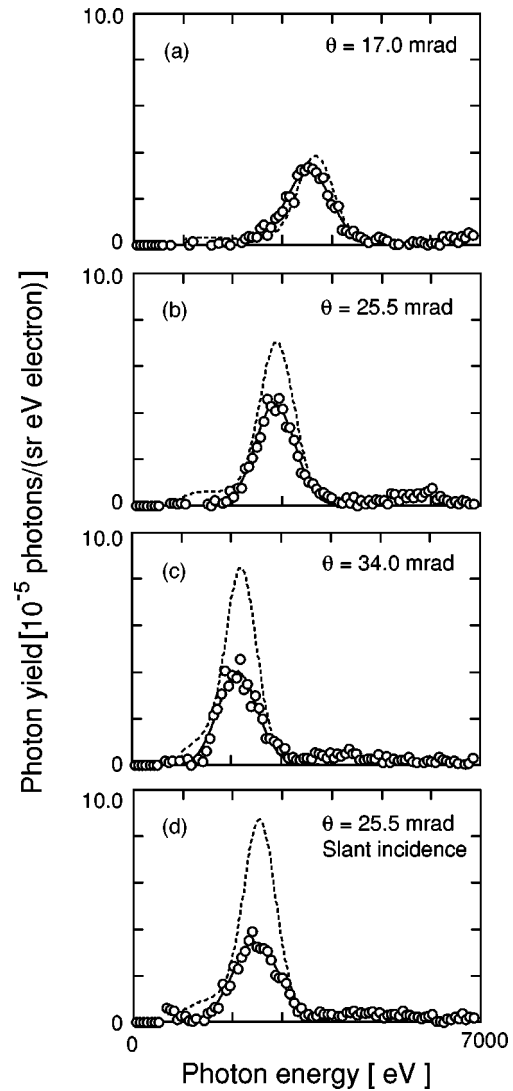


FIG. 8. Measured RTR spectra. The open circles and solid lines represent the experimental photon yields and their fitted Gaussian functions, respectively. The dotted lines represent the spectra of theoretical estimations. The error bars are not shown in these figures because their sizes are almost the same as that of the symbols.

rays from the multilayer target had a large peak around the 40th channel of the MCA, which represented nearly 3 keV. Its peak height was far larger than that of the background, which consisted of the bremsstrahlung and a negligible level of single-surface TR. The clear discrimination of the peak from the background means the peak is merely the RTR spectrum.

To analyze the measured spectra quantitatively, the raw spectra were converted to the differential photon yields per solid angle per electron. The photon yields from the multilayer target were subtracted the background yields and then were fitted on a Gaussian function as performed in the preceding section. The fitted results are listed in Table I, and the fitted curves are shown in Figs. 8(a)–8(c). The spectra of the theoretical estimations are also shown in these figures. The correlation coefficients in Table I, all of which are over 0.95, and the fitted curves in Fig. 8 show that the fitting is reliable.

As shown in Fig. 8, each spectrum has a single peak between 2 and 4 keV, which corresponds to our expected en-

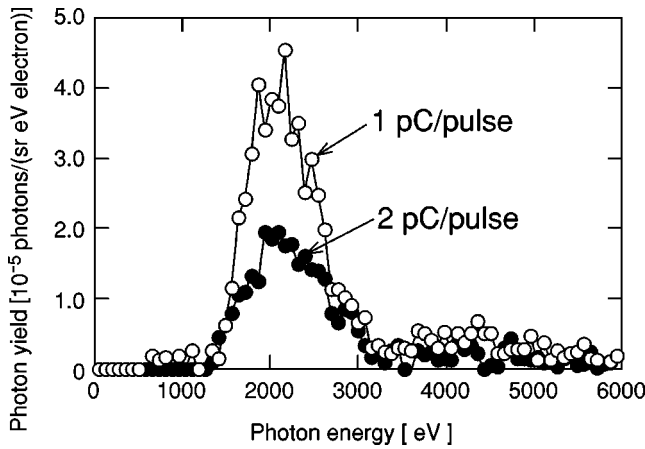


FIG. 9. Dependence of measured RTR spectra on the charge amount per beam pulse.

ergy region. Apparent higher harmonic peaks cannot be seen. The experimental results show that the peak energies depend on the observation angle. The shift of the peak energy agrees well with the theoretical estimations. The single-peaked spectra and the peak shift depending on the observation angle in these experiments can be evidence of single-mode RTR.

The measured bandwidths, represented by σ_ϵ , are 5–17% larger than those theoretically estimated. The extra broadening of the peak width mainly originates from the variations in the layer thickness. Referring to Eq. (A13) in the Appendix, the standard deviation of the phase error of 3.3% in our target reduces the peak height by about 92% of its ideal value. Assuming total yield is kept constant, this effect leads to an extra broadening of the peak width of about 8%, which, we think, agrees roughly with the measured extra broadening. The broadening due to the pile-up effects does not have to be considered here because all the events relating to the pile-up have been rejected by a gating circuit.

The absolute yield, represented by S_0 , of the 17-mrad experiment agrees exactly with the theoretical estimation. The exact agreement shows that no pile-up has occurred in this experiment. However, the ratio of the measured yield to the one theoretically estimated decreases as the observation angle becomes larger. The decrease of the yields in the 25.5- and 34.0-mrad experiments is mainly due to the pile-up effects. This assertion is supported by the fact that the event rate in these experiments should be about two times larger than that in the 17.0-mrad experiment. Serious pile-up effect was confirmed by an additional experiment in which the charge amount in a pulse was twice that in the normal condition. The spectrum observed in the additional experiment at the observation angle of 34.0-mrad is shown in Fig. 9. The doubling event rate greatly reduces the measured yield. Considering the exact agreement in the 17-mrad experiments and serious pile-up effect in the other two experiments, we conclude that the original yields in all of our experiments are essentially very close to the theoretical estimations.

B. Dependence on incident angle

We also observed the spectrum at an incident angle of 65° by rotating the target stage at the observation angle of 25.5 mrad. The measured data were fitted in the same manner as

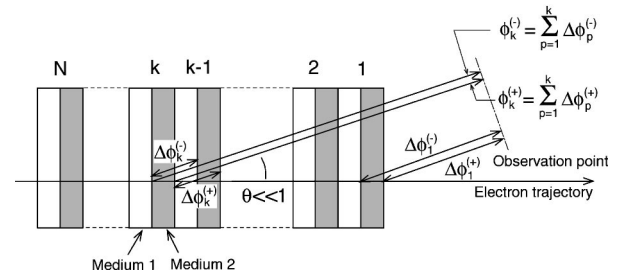


FIG. 10. Schematic of the resonance effect of TR in a multilayer target.

the previous experiments. The fitted results are listed in Table I, and the fitted curves are shown in Fig. 8(d). The peak energy of the spectrum at slant incidence is lower than that in normal incidence. The peak shift of about 390 eV is close to the theoretical estimation. The peak shifts depending on the incident angle can also be evidence of single-mode RTR. The bandwidth of the spectrum for the 65° incidence is broader than that in the normal incidence. This peak broadening might be due to an intermittent blow-up of LINAC beam emittance which occurred only in this experiment.

VI. CONCLUSION

We have observed single-mode resonant transition radiation in the soft-x-ray region by using a multilayer target with a submicrometer period. The measured spectra had a clear single peak at energies from 2 to 4 keV depending on the observation angle. The peak energy also depended on the incident angle of the electron beam. These experimental results apparently show the resonance effect of single-mode RTR. The experimental results also agreed quantitatively with the theoretical estimations involving the effect of spectral degradations. We thus conclude that these experimental results are evidence of single-mode RTR. To the best of our knowledge, these are the first experimental results confirming single-mode RTR.

Our success in observing single-mode RTR was due to the use of a Ni/C multilayer target with submicrometer period and medium-energy electron beams. The multilayer target was especially useful. Its effectiveness stems from the use of mature semiconductor technology to make uniform layers less than a micrometer thick.

ACKNOWLEDGMENT

We wish to thank the staff of Nihon-Meccs Corporation for helping us operate the LINAC during the experiments.

APPENDIX A: EFFECT OF ERRORS IN THE LAYER THICKNESS

We consider a multilayer structure consisting of N pairs of medium 1 with l_1 thickness and medium 2 with l_2 , as shown in Fig. 10. For simplicity, we assume here that the emission angle is small and the observation point is far from the target. Moreover, we assume that the absorption of the radiation in the target is negligible.

Modifying Eq. (A3) of Cherry [6], the field amplitude of RTR is expressed as follows:

$$E = E^{(+)} - E^{(-)} = E_0 \sum_{k=1}^N \exp \left\{ i \sum_{p=1}^k \Delta \phi_p^{(+)} \right\} - E_0 \sum_{k=1}^N \exp \left\{ i \sum_{p=1}^k \Delta \phi_p^{(-)} \right\}, \quad (\text{A1})$$

where E_0 is the field amplitude from one interface, and $\Delta \phi_p^{(\pm)}$ is the phase advance of the radiation passing through the p th layer pair. The superscripts $+$ and $-$ represent radiations generated at interfaces from medium 2 into 1 and from medium 1 into 2, respectively.

In the case of single mode resonance, the phase factors satisfy the following conditions:

$$\Delta \phi_1^{(\pm)} = \phi_0^{(\pm)} + 2\pi \delta_1^{(\pm)}, \quad (\text{A2})$$

$$\Delta \phi_p^{(\pm)} = 2\pi(1 + \delta_p^{(\pm)}), \quad (\text{A3})$$

$$\phi_0^{(-)} - \phi_0^{(+)} = \pi, \quad (\text{A4})$$

where $\delta_p^{(\pm)}$ represents the fractional phase error in the p th layer. Substituting these phase relations into Eq. (A1), we obtain

$$E^{(\pm)} = E_0 \exp(i\phi_o^{(\pm)}) \sum_{k=1}^N \exp \left\{ 2\pi i \left(\sum_{p=1}^{k-1} \delta_p^{(\pm)} + \delta_k^{(\pm)} \right) \right\}. \quad (\text{A5})$$

Since N is generally large, for most of all the k 's the summation in the exponential term of this equation should statistically be smaller than or comparable to the standard deviation of $\delta^{(\pm)}$. For the simple treatment of this summation, therefore, we assume

$$\sum_{p=1}^{k-1} \delta_p^{(\pm)} + \delta_k^{(\pm)} \cong \sqrt{2} \delta_k^{(\pm)}. \quad (\text{A6})$$

We thus obtain the following simplified equation for the radiation amplitude:

$$E^{(\pm)} \cong E_0 \exp(i\phi_o^{(\pm)}) \sum_{k=1}^N \exp\{2\sqrt{2}\pi i \delta_k^{(\pm)}\}. \quad (\text{A7})$$

The power of radiation, which is proportional to the photon number, is given by

$$P = \kappa E E^* = \kappa E_0^2 \left(\sum_{k=1}^N \sum_{l=1}^N \exp\{2\sqrt{2}\pi i(\delta_k^{(+)} - \delta_l^{(+)})\} + \sum_{k=1}^N \sum_{l=1}^N \exp\{2\sqrt{2}\pi i(\delta_k^{(+)} - \delta_l^{(-)})\} + \sum_{k=1}^N \sum_{l=1}^N \exp\{2\sqrt{2}\pi i(\delta_k^{(-)} - \delta_l^{(+)})\} + \sum_{k=1}^N \sum_{l=1}^N \exp\{2\sqrt{2}\pi i(\delta_k^{(-)} - \delta_l^{(-)})\} \right), \quad (\text{A8})$$

where κ is a constant and superscript $*$ represents the conjugate. Here we expand the exponential terms of Eq. (A8) into the second-order polynomials and then simplify the equation by using the following relations for statistical errors:

$$\sum_{k=1}^N \sum_{l=1}^N \delta_k^{(\pm)} \delta_l^{(\pm)} \cong \sum_{k=1}^N \delta_k^{(\pm)2}, \quad (\text{A9})$$

$$\sum_{k=1}^N \sum_{l=1}^N \delta_k^{(+)} \delta_l^{(-)} \cong 0. \quad (\text{A10})$$

We thus obtain the power of radiation as

$$P \cong 4\kappa E_0^2 \left[N^2 - 2(2N-1)\pi^2 \left\{ \sum_{k=1}^N \delta_k^{(+2)} + \sum_{k=1}^N \delta_k^{(-2)} \right\} \right]. \quad (\text{A11})$$

Dividing Eq. (A11) by the power without phase errors and rewriting the summations as

$$\sum_{k=1}^N \delta_k^{(\pm)2} \cong N \sigma_\delta^{(\pm)2}, \quad (\text{A12})$$

where $\sigma_\delta^{(\pm)}$ is the standard deviation of phase errors, we obtain the ratio of the degraded radiation power to its ideal value as follows:

$$\frac{P}{P_{\text{ideal}}} \cong 1 - \frac{2(2N-1)}{N} \pi^2 \{ \sigma_\delta^{(+2)} + \sigma_\delta^{(-2)} \}. \quad (\text{A13})$$

[1] G. M. Garibian, Zh. Éksp. Teor. Fiz. **33**, 1403 (1957) [Sov. Phys. JETP **6**, 1079 (1958)].
 [2] M. A. Piestrup, J. O. Kephart, H. Park, R. K. Klein, R. H. Pantell, P. J. Ebert, M. J. Moran, B. A. Dahling, and B. L. Berman, Phys. Rev. A **32**, 917 (1985).
 [3] M. L. Ter-Mikaelyan, Nucl. Phys. **24**, 43 (1961).
 [4] H. Backe, S. Gampert, A. Grendel, F.-J. Hartmann, W. Lauth, Ch. Weinheimer, R. Zahn, F. R. Buskirk, H. Euteneuer, K. H. Kaiser, G. Stephan, and Th. Walcher, Z. Phys. A **349**, 87 (1994).

[5] T. Tanaka, T. Awata, A. Itoh, N. Imanishi, T. Yamakawa, M. Yamada, S. Urasawa, and T. Nakazato, Nucl. Instrum. Methods Phys. Res. B **93**, 21 (1994).
 [6] M. L. Cherry, G. Hartmann, D. Müller, and T. A. Prince, Phys. Rev. D **10**, 3594 (1974).
 [7] X. Artru, G. B. Yodh, and G. Mennessier, Phys. Rev. D **12**, 1289 (1975).
 [8] M. J. Moran, B. A. Dahling, P. J. Ebert, M. A. Piestrup, B. L. Berman, and J. O. Kephart, Phys. Rev. Lett. **57**, 1223 (1986).

- [9] B. L. Henke, E. M. Gullikson, and J. C. Davis, *At. Data Nucl. Data Tables* **54**, 2 (1993). *Proceedings of the 1989 IEEE Particle Accelerator Conference*, edited by F. Bennett and J. Kopta (IEEE, Chicago, 1989), p. 1459.
- [10] T. Hosokawa, *Synch. Radiat. News* **6**, 16 (1993).
- [11] T. Hosokawa, T. Kitayama, T. Hayasaka, S. Ido, Y. Uno, A. Shibayama, J. Nakata, K. Nishimura, and M. Nakajima, in *Proceedings of the 1989 IEEE Particle Accelerator Conference*, edited by F. Bennett and J. Kopta (IEEE, Chicago, 1989), p. 1459.
- [12] A. C. Huber, J. A. Pantazis, and V. Jordanov, *Nucl. Instrum. Methods Phys. Res. B* **99**, 665 (1994).